

Evaluation of the Utility of Satellite-Based Vegetation Leaf Area Index Data for Climate Simulations

WOLFGANG BUERMANN AND JIARUI DONG

Department of Geography, Boston University, Boston, Massachusetts

XUBIN ZENG

Institute of Atmospheric Physics, The University of Arizona, Tucson, Arizona

RANGA B. MYNENI

Department of Geography, Boston University, Boston, Massachusetts

ROBERT E. DICKINSON

School of Earth and Atmospheric Sciences, Georgia Institute of Technology, Atlanta, Georgia

(Manuscript received 21 August 2000, in final form 23 February 2001)

ABSTRACT

In this study the utility of satellite-based leaf area index (LAI) data in improving the simulation of near-surface climate with the NCAR Community Climate Model, version 3 (CCM3), GCM is evaluated. The use of mean LAI values, obtained from the Advanced Very High Resolution Radiometer Pathfinder data for the 1980s, leads to notable warming and decreased precipitation over large parts of the Northern Hemisphere lands during the boreal summer. Such warming and decreased rainfall reduces discrepancies between the simulated and observed near-surface temperature and precipitation fields. The impact of interannual vegetation extremes observed during the 1980s on near-surface climate is also investigated by utilizing the maximum and minimum LAI values from the 10-yr LAI record. Surface energy budget analysis indicates that the dominant impact of interannual LAI variations is modification of the partitioning of net radiant energy between latent and sensible heat fluxes brought about through changes in the proportion of energy absorbed by the vegetation canopy and the underlying ground and not from surface albedo changes. The enhanced latent heat activity in the greener scenario leads to an annual cooling of the earth land surface of about 0.3°C, accompanied by an increase in precipitation of 0.04 mm day⁻¹. The tropical evergreen forests and temperate grasslands contribute most to this cooling and increased rainfall. These results illustrate the importance and utility of satellite-based vegetation LAI data in simulations of near-surface climate variability.

1. Introduction

The importance of vegetation control on the exchange of energy, mass, and momentum between the land surface and the atmosphere has been the focus of several efforts (Betts and Beljaars 1993; LeMone et al. 2000; Sellers et al. 1995; Shuttleworth et al. 1991; among others). Many field experiments at different spatial and temporal scales have been conducted to test the sensitivity of climate to changes in land surface conditions (e.g., Bastable et al. 1993; Betts et al. 1996, 1999; Schwartz and Karl 1990). Their findings and results

from model investigations, recently summarized in Pielke et al. (1998), indicate that the effect of vegetation dynamics on climate might not be insignificant compared to other forcings resulting from changes in atmospheric composition, ocean circulation, and orbital perturbations.

In many studies involving atmospheric general circulation models (GCMs), a “case” simulation is typically performed with modified land surface characteristics and then compared with a “control” simulation. Such sensitivity studies have identified the significance of key land surface parameters such as albedo (Sud and Fennessey 1982), evapotranspiration (Shukla and Mintz 1982), surface roughness (Sud et al. 1988), and stomatal conductance (Henderson-Sellers et al. 1995; Pollard and Thompson 1995; Sellers et al. 1996; Martin et al. 1999) on land–atmosphere exchange processes. Model inves-

Corresponding author address: Wolfgang Buermann, Department of Geography, Boston University, 675 Commonwealth Ave., Boston, MA 02215.

E-mail: buerman@bu.edu

tigations with changes in global leaf area index (LAI; Chase et al. 1996) and replacement of entire biomes at regional [tropical in the case of Dickinson and Henderson-Sellers (1988); Lean and Warrilow (1989); Nobre et al. (1991); Zhang et al. (1996a,b); and boreal in the case of Bonan et al. (1992); Chalita and Le Treut (1994)] and global (Kleidon et al. 2000) scale indicate dramatically the importance of vegetation on regional and global climate.

The successful implementation of the role of vegetation in climate modeling requires credible specification of the numerical parameters needed by the underlying theory. Vegetation characteristics can either be prescribed or modeled as a component of the system. In either case, global-scale measurements are crucial, either for the model boundary conditions, similar to SSTs, or as means to validate modeled characteristics.

One focus of this study is to evaluate the feasibility of improving the simulated climate of the 1980s through the use of satellite-based LAI fields. Two GCM "experiments" were performed—a control and a simulation run in which the standard LAI values are replaced with climatological LAI data from the 10-yr monthly Pathfinder LAI dataset (Buermann et al. 2001, manuscript submitted to *J. Geophys. Res.*, hereinafter BWDZ) and the simulated near-surface temperature and precipitation fields over land are compared with observations. The climate simulations used the Community Climate Model (CCM3; Kiehl et al. 1996, 1998), with the Land Surface Model (LSM; Bonan 1996) as the associated land model, both developed at the National Center for Atmospheric Research (NCAR). Although CCM3 is in many respects a state-of-the-art general circulation climate model, it suffers from a cold bias in its simulation of near-surface land temperatures. Hence, it is of interest to explore the dependence of these temperatures on the model parameters used.

Hutjes et al. (1998) recently argued that one of the most important outstanding aspect in biosphere-atmosphere interactions is natural variability, particularly with respect to seasonal to interannual cycles. In this study, we attempt to quantify the impact of observed interannual variability in vegetation dynamics on near-surface climate during the 1980s. To do so, we conducted two GCM experiments in which minimum and maximum LAI values from the 10-yr LAI record were employed and then the differences in the simulated near-surface climates were analyzed.

2. Modeling impacts on climate from changes in LAI

a. Model description

In our investigations, we employed the general circulation model CCM3, which represents an upgraded version of CCM2 with improvements in parameterization of cloud properties, clear-sky longwave radiation,

deep convection, and boundary layer processes (Kiehl et al. 1996, 1998). LSM is an one-dimensional model of energy, momentum, water, and CO₂ exchange between the atmosphere and land (Bonan 1996). It solves for the vegetation and ground temperatures that balance the surface energy budget, taking into account ecological differences among vegetation types, hydraulic, and thermal differences among soil types and allowing for multiple plant types (up to three) within a vegetated model grid cell. The model evaluates surface fluxes at every time step (20 min) and for each subgrid cell independently, using the same grid-averaged atmospheric forcing. It then provides the grid-averaged surface fluxes to the atmosphere by taking into consideration the subgrid fractional areas.

b. Processes in the LSM impacted by LAI changes

The LSM distinguishes 13 unmixed plant types, which differ in leaf and stem area, leaf optical properties, leaf dimensions, roughness length, stomatal physiology, and root profile (Bonan 1996). In this model, changes in LAI directly affect evapotranspiration and surface albedo of the vegetated land surface.

Land surface evapotranspiration is subdivided into evaporation from wet leaf surfaces, transpiration from leaves, and evaporation from the soil. The wetness of leaves, that is, the interception storage capacity, is a direct function of LAI, leading to enhanced plant evaporation as LAI increases. Canopy stomatal conductance is simulated through a physiology-based formulation, similar to Collatz et al. (1991) and Sellers et al. (1992), whose magnitude is controlled by prescribing values for the maximum photosynthesis parameter V_{\max} . It is coupled to leaf stomatal physiology and the amount of absorbed photosynthetically active radiation (APAR) for both sunlit and shaded portions of the canopy. APAR is determined by plant-specific structural and optical properties. Generally, with increasing LAI under optimal growing conditions, enhanced canopy conductance, and plant evaporation will cause the latent heat flux to increase. Further, the intensified transport of moisture to the atmosphere could enhance precipitation and favor cloud development. This in turn could impact the surface energy balance by reducing the amount of incident solar radiation.

The surface albedo of a vegetated area in the LSM is computed with a two-stream approximation (Dickinson 1983; Sellers 1985) and is a function of plant-specific structural and optical properties and LAI. Generally, surface albedo decreases as LAI increases due to increased canopy absorption and decreased reflection from the generally brighter ground below the vegetation. This is particularly true for snow-covered surfaces, where changes in LAI directly affect the fraction of canopy covered by snow in the model. Likewise, the surface albedo of sparsely vegetated areas (LAI < 1) may be sensitive to LAI changes. The LAI changes in

LSM, however, do not change either vegetation roughness length or fractional coverage so that elsewhere LAI-induced changes are expected to be small.

In summary, LAI changes in our simulations directly affect net solar radiation and the partitioning between latent and sensible heat. The key variables are canopy stomatal conductance, interception storage, and surface albedo. Cloud cover feedback indirectly affects net solar radiation through modifications to the incident solar flux.

c. LAI input to the LSM

In this study, we used a global LAI dataset of 0.25° spatial resolution. The data span the period July 1981–June 1991 at monthly interval. The LAI fields were derived from maximum NDVI value global composites of the National Oceanic and Atmospheric Administration–National Aeronautics and Space Administration Pathfinder Advanced Very High Resolution Radiometer (AVHRR) Land dataset, utilizing an algorithm that incorporates results from a three-dimensional radiative transfer model and a six-biome classification scheme as described in Myneni et al. (1997). Results from a recent analysis of this dataset indicate that variations in the LAI fields correspond well to El Niño–Southern Oscillation–related SST and rainfall anomalies in tropical and in some extratropical regions. In the northern high latitudes, trends and variations in LAI correlate significantly with near-surface spring and, to a lesser extent, summer temperatures. The consistent pattern among the independently derived datasets suggests that the LAI dataset is a reliable indicator of interannual vegetation dynamics (BWDZ).

The LSM employs prescribed biome-specific monthly LAI that are spatially invariant over an entire hemisphere. The radiative transfer biome map (Myneni et al. 1997) was converted to the 13 LSM vegetation types using Olson's land cover map (Olson et al. 1983) and latitudinal information. The satellite LAI fields were then aggregated by LSM vegetation types and allowed for changes between the two hemispheres, shifting LAI by 6 months as in Bonan (1996). For each month and each LSM vegetation type, average, minimum and maximum LAI values were determined based on the 10-yr LAI record.

In Fig. 1, these LAI profiles are shown along with the LSM standard profiles. The satellite LAI profiles show gradual monthly variations and a general lag in phase when compared with the LAI profile in the LSM. For several biome types, the satellite LAI values are considerably lower than those used in the LSM. Among the most abundant of these are cool and warm grass, needle leaf evergreen tree, arctic grass, crop, and broadleaf evergreen tree. Monthly maximum and minimum LAI values also differ notably. In the case of trees, these LAI differences can be as large as 2. In the case of broadleaf evergreen tree, the minimum LAI values ap-

pear to be low, possibly indicating residual cloud contamination problems in the satellite data. In the case of needleleaf evergreen tree, very low LAI values during the winter season were observed in the satellite dataset. This is an artifact mainly associated with lack of valid wintertime data from snow-covered vegetation, low sun angles, and a temperature threshold (0°C) in the LAI retrieval algorithm. These profiles were improved in an ad hoc manner, such that the minimum value during winter was not less than 80% of the maximum summer value.

d. Model runs

In this study, the NCAR CCM3 (Kiehl et al. 1996) with online LSM (Bonan 1996) was run at the standard T42 resolution (approx $2.8^\circ \times 2.8^\circ$). Four 10-yr model runs were performed, changing the monthly LAI profiles in the LSM. The runs are designated as (a) control, (b) meanLAI, (c) minLAI, and (d) maxLAI (Fig. 1). Each run was started in July 1981, utilizing observed inter-annually varying sea surface temperatures (SSTs). This particular time frame was chosen to be consistent with the monthly record for which satellite LAI fields were available. Initial conditions for the control run (temperature, snow, soil water, etc.) were obtained from July of year 10 from a 10-yr simulation that used climatological SSTs. For the satellite LAI (meanLAI, minLAI, and maxLAI) runs, initial conditions were extracted from July of year 10 from a 10-yr simulation employing satellite-derived mean LAI fields (Fig. 1) and climatological SSTs.

The choice of this particular 10-yr time period (Jul 1981–Jun 1991) for the model runs, though, leads to the fact that for the season June–August (JJA) and the annual case only 9 yr of data for each grid cell are available. Consequently, in this study all JJA and annual means are based on 9 yr (1982–90), whereas all DJF means are based on 10 yr (1981/82–1990/91). We could have chosen to use also 9 yr of data for the DJF means (1982/83–1990/91) to make the averaging periods consistent, but then would have discarded one year of data.

In order to evaluate possible effects of spinup resulting from differing initial conditions in the actual control and satellite LAI runs, we repeated the analysis with varying averaging periods: last 8 yr (DJF), last 7 yr (JJA and annual), and last 5 yr (for all means). The results, not shown, indicate no apparent drifts or trends in the temporal means, suggesting that the initial conditions that were provided to the actual runs represented equilibrium states. Hence, differing initial conditions are not expected to be responsible for portion of the multiyear mean differences between the control and satellite LAI runs.

3. Results and analysis

a. Mean LAI versus control simulation

Previously, Bonan (1998) compared results from a CCM3–LSM standard simulation with observed near-

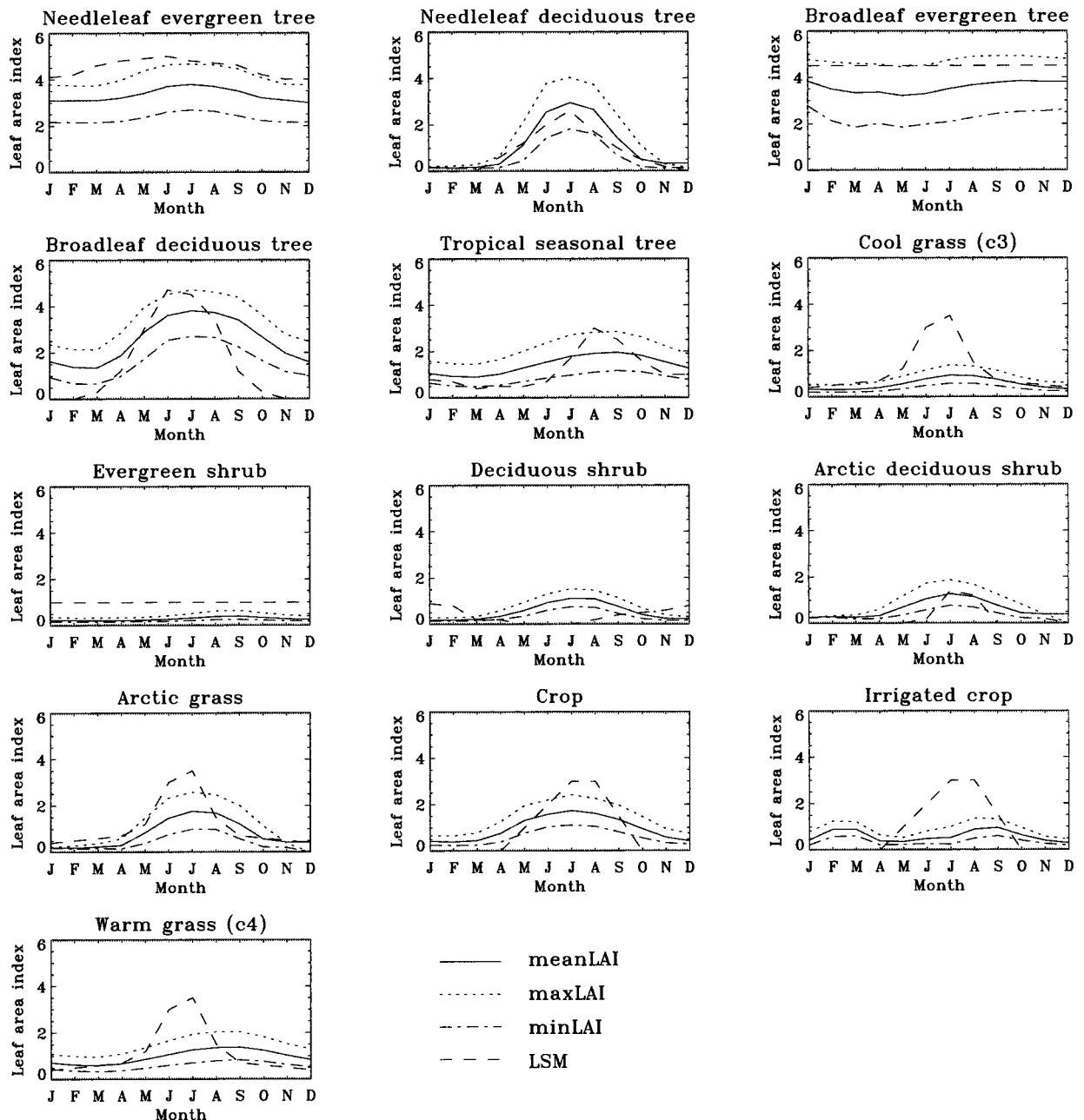


FIG. 1. Comparison of Northern Hemisphere LSM vegetation-type LAI profiles. Mean, maximum, and minimum LAI profiles were derived from the AVHRR Pathfinder NDVI data as described in BWDZ. The LSM profiles are also shown.

surface temperatures and precipitation. The simulations were colder by about 2.5° – 5.0° C with respect to the observed temperatures over much of Asia and northern Europe during the boreal summer period. Furthermore, simulated precipitation in the northern high-latitude regions was found to be consistently overestimated. In this section, we assess the possibility of reducing the model biases in temperature and precipitation if satellite LAI fields were to be used instead of the LSM fields. We first present the differences between the two LAI

data, followed by a comparison of the simulated temperature and precipitation fields with observations.

1) DIFFERENCES IN LAI

In the LSM, vegetated regions are designated according to 26 surface types. Each of these accommodate up to three different vegetation types and/or bare ground (Bonan 1996). A map of 10-yr average satellite LAI for each LSM surface type ($2.8^{\circ} \times 2.8^{\circ}$) was generated with

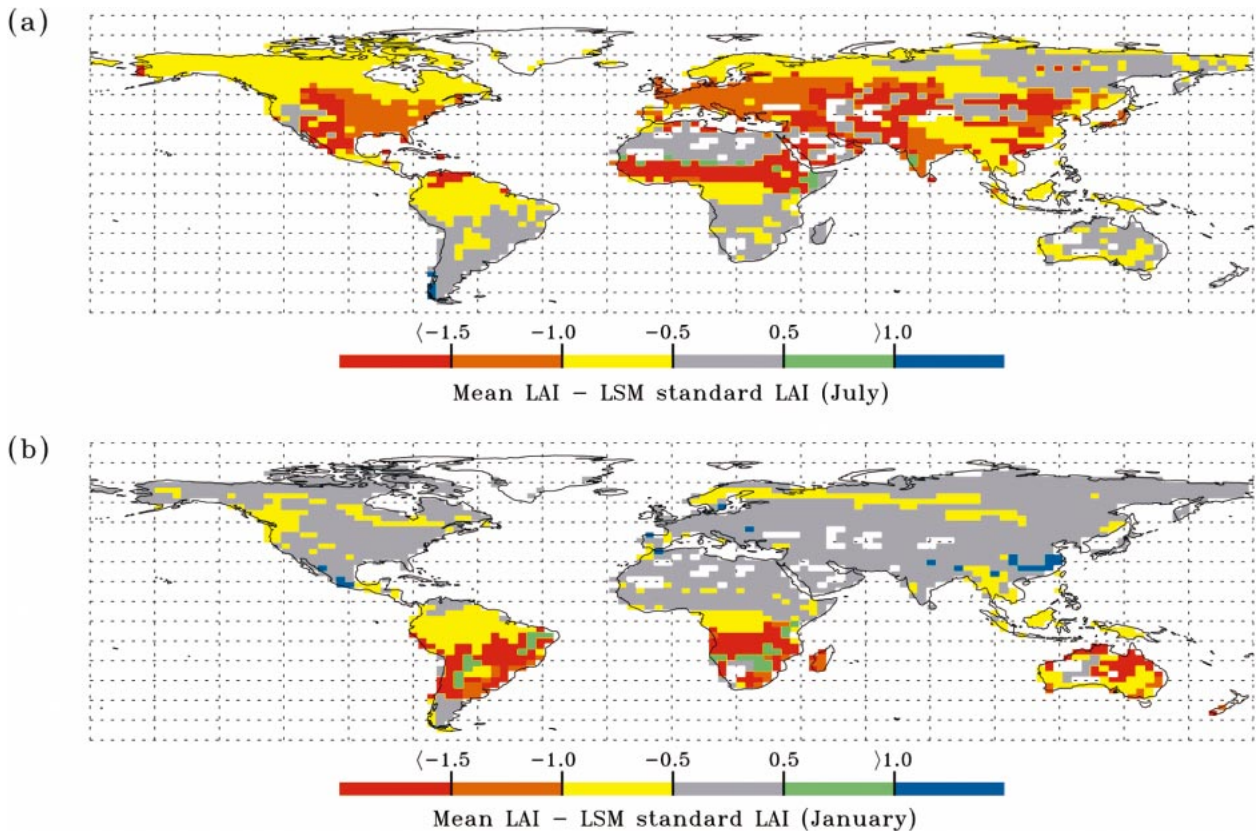


FIG. 2. Spatial pattern of the difference between mean satellite and LSM LAI data for (a) Jul and (b) Jan.

the mean LAI profiles shown earlier (Fig. 1). Figure 2 shows the geographical distribution of the differences between the average satellite and the LSM standard LAI fields for July and January. Large LAI differences (>1.5) can be seen in July in the central United States, sub-Saharan Africa, and in Eurasia. These can be attributed to LSM vegetation types cool and warm grass. For these, the LSM LAI fields are overestimates compared to the satellite data (Fig. 1). Elsewhere in these regions, differences of about 1.0–1.5 LAI are mostly in areas where crops and broadleaf deciduous vegetation predominate. In the Southern Hemisphere and in the northern high latitudes, the differences between the two are minor. In the month of January, however, significant LAI differences (>1.5) are seen in the warm grass lands of the Southern Hemisphere. Overall, the satellite LAI estimates are lower in magnitude than the LSM prescriptions in both the hemispheres during the respective growing seasons and this, all else remaining the same, should result in reduced latent heat flux and warmer near-surface climate.

2) COMPARISON WITH OBSERVATIONS

For purposes of evaluating the simulations, we use the monthly near-surface temperature data from Jones et al. (1999) and the monthly precipitation data from

Hulme et al. (1998) gridded to $2.8^\circ \times 2.8^\circ$ resolution and averaged over the period of model runs (Jul 1981–Jun 1991). In Figs. 3a and 3c, the spatial distribution of the differences in near-surface temperature between the control run and observations are shown for the boreal (JJA) and austral summers (DJF). The patterns are nearly identical to those from a 15-yr control run (1979–93) reported previously by Bonan (1998). Comparing these with the results from the satellite LAI (meanLAI) and control runs allows for an evaluation of the utility of satellite LAI (Figs. 3b and 3d). The obvious improvement is warming in the satellite LAI simulation during JJA over large parts of the Northern Hemisphere lands, which partly offsets the previously mentioned cold bias in the control LSM simulation. Notably, warming is seen over the grasslands of western Asia ($>1.6^\circ\text{C}$), southern Africa ($>1.3^\circ\text{C}$), and the central United States ($>1.1^\circ\text{C}$). This warming is mainly due to the lower magnitude of satellite LAI data for the vegetation types present here (Fig. 2a). The large-scale cooling in northern Asia adds to the existing cold bias. In the austral summer (DJF), simulation improvements are evident over large parts of Australia, Africa, South America, and far east Asia. The northern high latitudes show a significant cooling of up to 3.0°C in Eurasia and 2.0°C in North America, which improves the simulation but still overestimates the observed station temperature

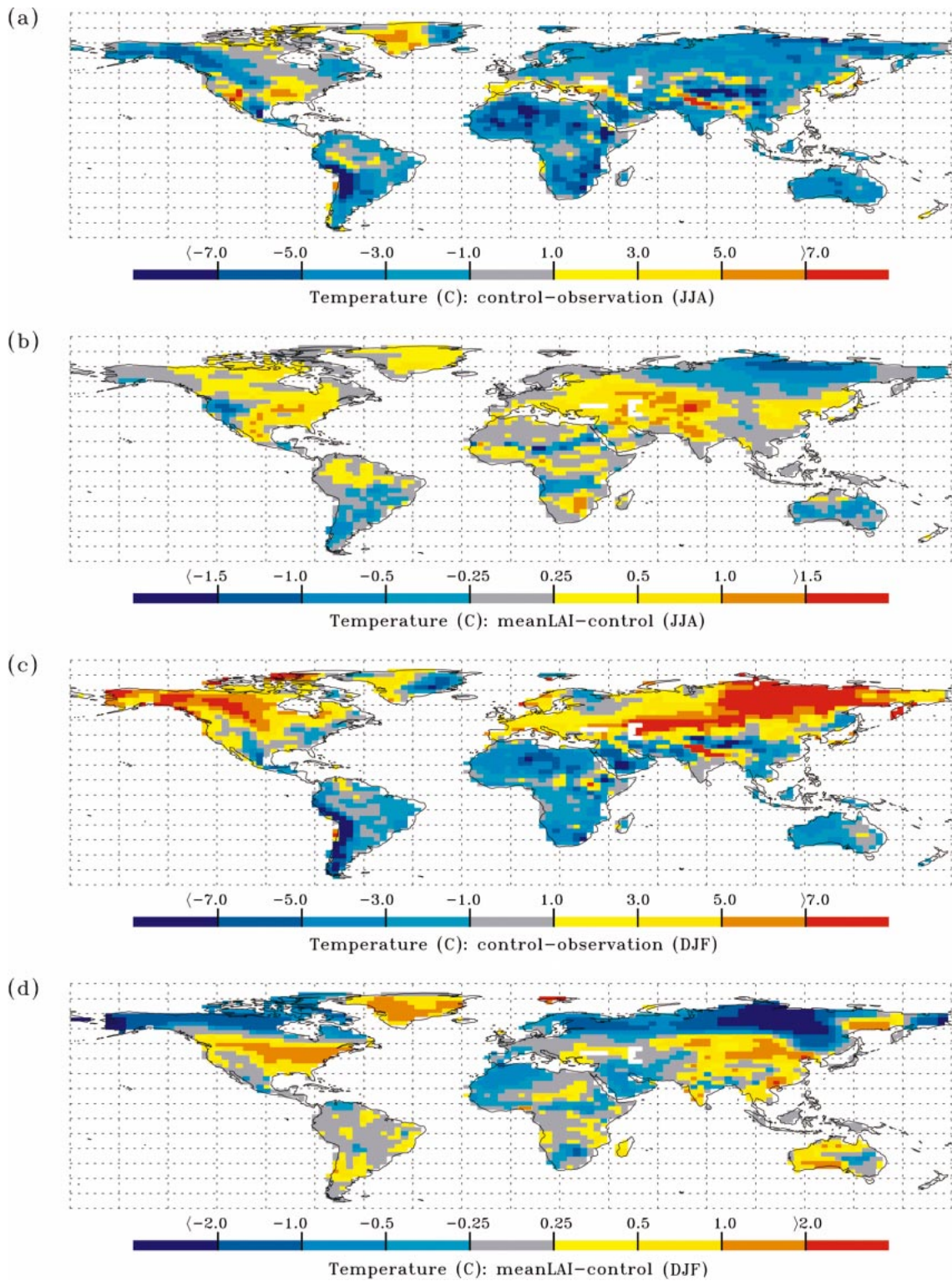


FIG. 3. Spatial pattern of the seasonal difference in mean near-surface temperature: (a) control - observed in JJA, (b) meanLAI - control in JJA, (c) control - observed in DJF, and (d) meanLAI - control in DJF. Simulated and observed temporal means are based on 9 yr for JJA (1982-90) and 10 yr for DJF (1981/82-1990/91), respectively. Observed temperature data are from Jones et al. (1999).

TABLE 1. Simulated and observed (Jones et al. 1999) near-surface temperature (2-m height) by LSM surface type, season, and latitudinal band. Simulated and observed temporal means are based on 9 yr for JJA and the annual case (1982–90) and 10 yr for DJF (1981/82–1990/91).

Season	LSM surface type	Zonal band (No. of pixel)	Temperature (°C)				Observed
			Control	Case minus control			
				Min*	Mean*	Max*	
JJA	Warm grassland	40°–60°N (40)	19.23	+0.84	+0.92	+0.14	20.12
		23°–40°N (88)	24.69	+0.68	+0.61	+0.26	26.03
		0°–23°N (39)	26.03	+0.61	+0.27	+0.2	29.21
		23°S–0° (38)	18.44	+0.01	–0.26	–0.54	21.72
		60°–23°S (40)	9.41	–0.13	–0.37	–0.47	13.19
		60°–80°N (7)	9.51	+0.35	–0.09	–0.09	13.01
	Cool grassland	40°–60°N (56)	16.18	+0.62	+0.58	–0.21	18.28
		23°–40°N (6)	10.93	+0.47	+0.10	–0.20	13.74
		40°–60°N (64)	15.40	+0.48	+0.38	–0.12	16.48
	Cool forest crop	40°–60°N (34)	17.72	+0.93	+0.52	–0.20	18.49
	Cool crop	60°–80°N (12)	11.69	+0.01	+0.39	–0.26	14.09
	Cool mixed NET**/BDT**	40°–60°N (30)	13.57	+0.34	+0.13	–0.01	14.77
DJF	Warm grassland	40°–60°N (40)	–5.02	+0.19	+0.33	+0.07	–7.87
		23°–40°N (88)	5.37	–0.01	–0.01	–0.23	8.01
		0°–23°N (39)	21.09	0.00	–0.05	–0.43	23.36
		23°S–0° (38)	22.39	+0.52	+0.27	+0.04	25.70
		60°–23°S (40)	21.82	+0.34	+0.25	–0.21	24.29
		60°–23°S (31)	25.64	+0.26	+0.36	–0.29	25.81
Annual	Evergreen shrubland	0°–23°N (69)	23.29	+0.43	+0.14	–0.06	24.80
	Tropical BET	23°S–0° (78)	24.28	+0.59	+0.13	–0.08	25.80

* Min, Mean, and Max indicate MinLAI, MeanLAI, and MaxLAI runs, respectively.

** NET, BDT, and BET indicate needleleaf evergreen tree, broadleaf deciduous tree, and broadleaf evergreen tree, respectively.

data. It is interesting to note that the observed cooling here is very little associated with direct LAI forcing at this time of year (Fig. 2b). It is possible that changes in LAI forcing in the Tropics or midlatitudes affect the winter near-surface climate in the high latitudes through changes in large-scale atmospheric circulation (Chase et al. 1996; see also next section).

Table 1 lists the LSM surface types for which consistent improvements in temperature simulation are seen when the standard LSM LAI profiles are replaced by the satellite profiles. The most prominent are the LSM surface types warm and cool grasslands which have large fractional coverage of warm and cool grasses. Both vegetation types have substantially lower satellite LAI values (about 2.5) during the growing season (Fig. 1). These decreases in LAI generally cause surface albedos to increase, which should lead to cooler surface temperatures. However, it appears that the near-surface climate at these sites is much more influenced by decreased evapotranspiration, leading to the observed warmer temperatures. The minimum LAI (minLAI) and maximum LAI (maxLAI) entries denote the bounds of LAI impact on temperature, which is discussed in the next section. It should be noted that even though satellite LAI helps to reduce cold biases in near-surface temperature over certain regions other processes in the atmosphere or prescribed surface albedo for bare soil and thick canopy (stomatal resistance too small) might be primarily responsible for the bias on the global scale.

Figures 4a and 4c show the spatial distribution of the differences in total precipitation between the control run

and observations for the boreal (JJA) and austral (DJF) summers. Total precipitation in the northern high-latitude regions and the Tibetan Plateau is consistently overestimated in the control run for both seasons. During the austral summer, large regions in the Southern Hemisphere also receive excessive rainfall. In Figs. 4b and 4d, the differences in total precipitation between the satellite LAI and control simulation for the two seasons are shown. During the boreal summer, less rainfall in the northern high latitudes (>0.7 mm day^{–1}) and over the Tibetan Plateau (>0.8 mm day^{–1}) in the satellite LAI simulation lowers the discrepancies. As discussed above, the lower magnitude of satellite LAI reduces evapotranspiration and, consequently, precipitation (Fig. 2a). During the austral summer, simulation improvements can also be seen over large parts of Australia, Africa, South America, and high-latitude regions of Asia.

b. Interannual variability

Here we present results from a near-surface climate and energy budget analysis from two simulations, denoted as minLAI and maxLAI, which correspond respectively to simulations with minimum and maximum satellite LAI profiles shown in Fig. 1. These correspond to the observed variability during the 1980s. The goal of this analysis is to gain insight on the possible impact of vegetation dynamics on near-surface climate at interannual scales. It should be noted that simulations with these profiles correspond effectively to assuming that

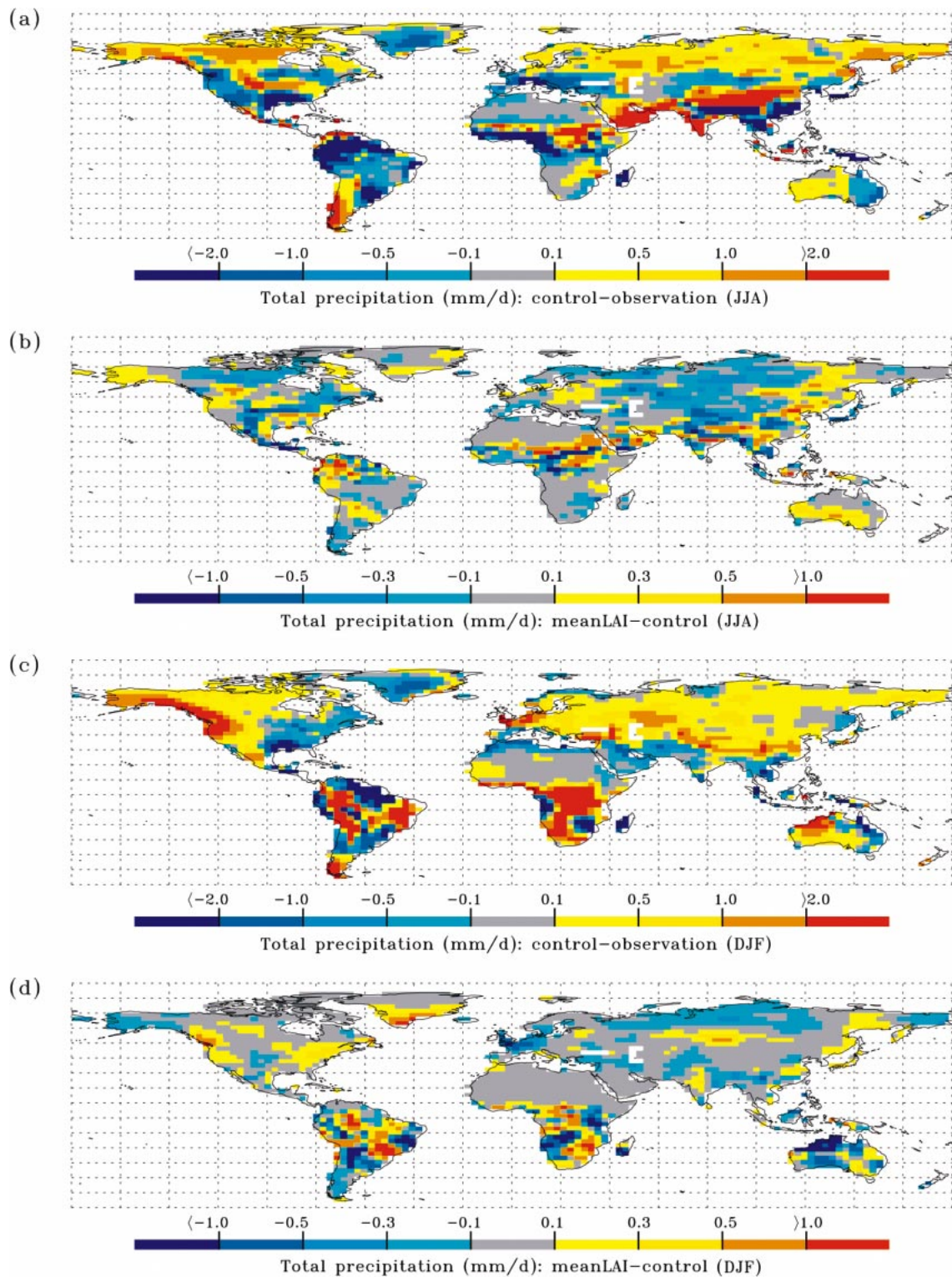


FIG. 4. Spatial pattern of the seasonal difference in mean total precipitation: (a) control - observed in JJA, (b) meanLAI - control in JJA, (c) control - observed in DJF and (d) meanLAI - control in DJF. Simulated and observed temporal means are based on 9 yr for JJA (1982-90) and 10 yr for DJF (1981/82-1990/91), respectively. Observed precipitation data are from Hulme et al. (1998).

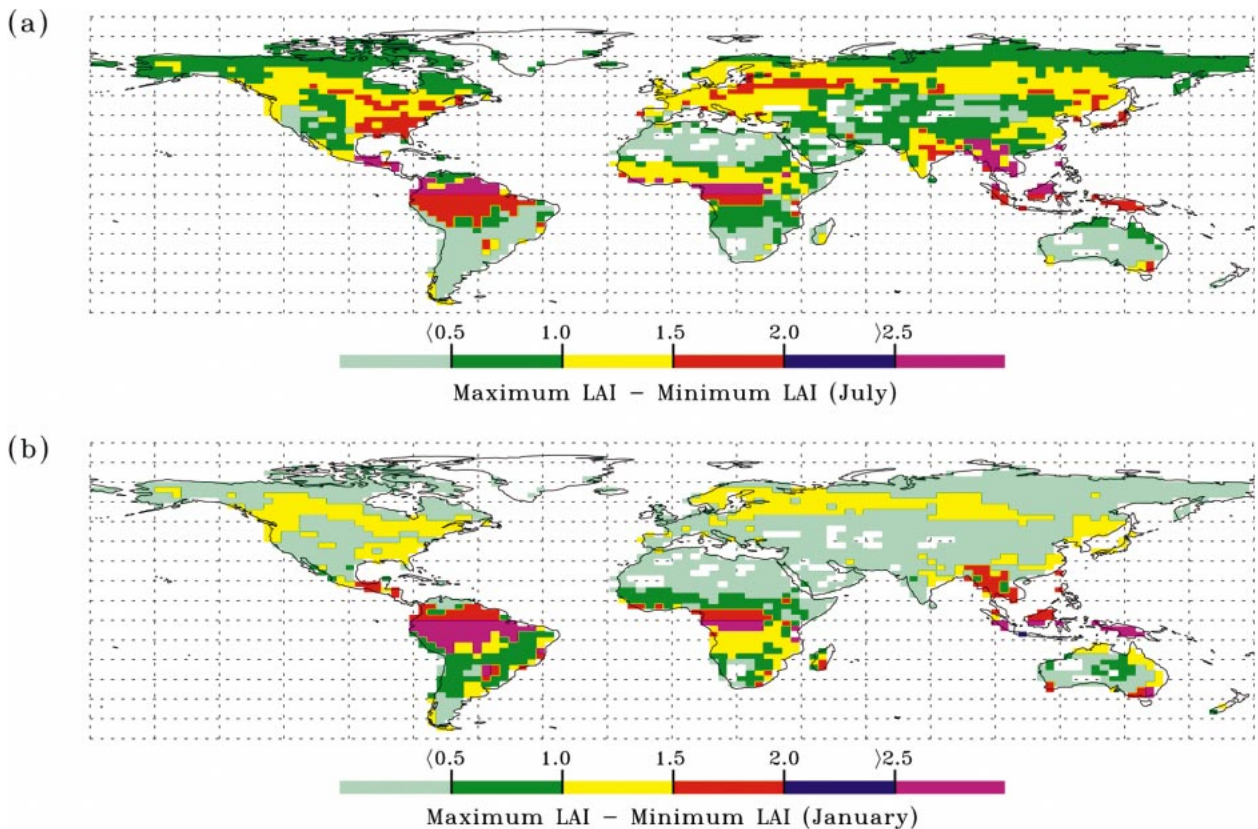


FIG. 5. Spatial pattern of the difference between maximum and minimum satellite LAI fields for (a) Jul and (b) Jan.

all the vegetation types experienced either the minimum or maximum LAI everywhere at the same time, which clearly is not realistic. Hence, the value of these simulations is in possibly being able to derive an estimate that brackets the impacts of interannual LAI changes on near-surface climate. We first discuss the satellite LAI fields and then present results at regional and global scales.

1) VEGETATION EXTREMES DURING THE 1980s

Maps of LAI extremes for each LSM surface type ($2.8^\circ \times 2.8^\circ$) were generated with the minimum and maximum LAI profiles shown earlier (Fig. 1). They illustrate the range of LAI variations observed during the July 1981 to June 1991 period. Figure 5 shows the global distribution of the difference between maximum and minimum LAI for the months of July and January, respectively. In July, large areas in the Northern Hemisphere show LAI differences greater than 1.0, indicating significant interannual variability in vegetation greenness during the active growing season. Differences greater than 1.5 are notable in the eastern United States and central Europe where the LSM surface types with significant tree fractions exist (e.g., cool forest crop). Similarly, large LAI changes can be seen in the Tropics year-round. These figures illustrate an extreme reali-

zation of the extent of interannual variability in vegetation greenness during the 1980s, because not all regions experienced the minimum (or maximum) values simultaneously. The value of these constructs, then, is their utility in possibly deriving the upper and lower bounds of the impact on climate.

2) SPATIAL AND SEASONAL DIFFERENCES

Figures 6 and 7 show the spatial pattern of surface climatic variables as differences between the maxLAI and minLAI simulation during the Northern (JJA) and Southern (DJF) Hemisphere summer seasons, respectively. The increase in JJA latent heat flux over large vegetated temperate areas of North America and Eurasia is evident in the maxLAI simulation (Fig. 6b). In particular, the grass- and croplands in the midlatitudes of Eurasia show marked increases, sometimes in excess of 15 W m^{-2} . In DJF, similar changes in latent heat flux can be observed in all the three southern continents (Fig. 7b). These patterns correspond well to the LAI changes shown previously in Fig. 5, clearly indicating the importance of vegetation control on surface latent heat flux. Furthermore, it appears that the impact of LAI change on the magnitude of latent heat flux is larger in the case of vegetation types with low average LAI, as for example grasses, possibly due to the nonlinear de-

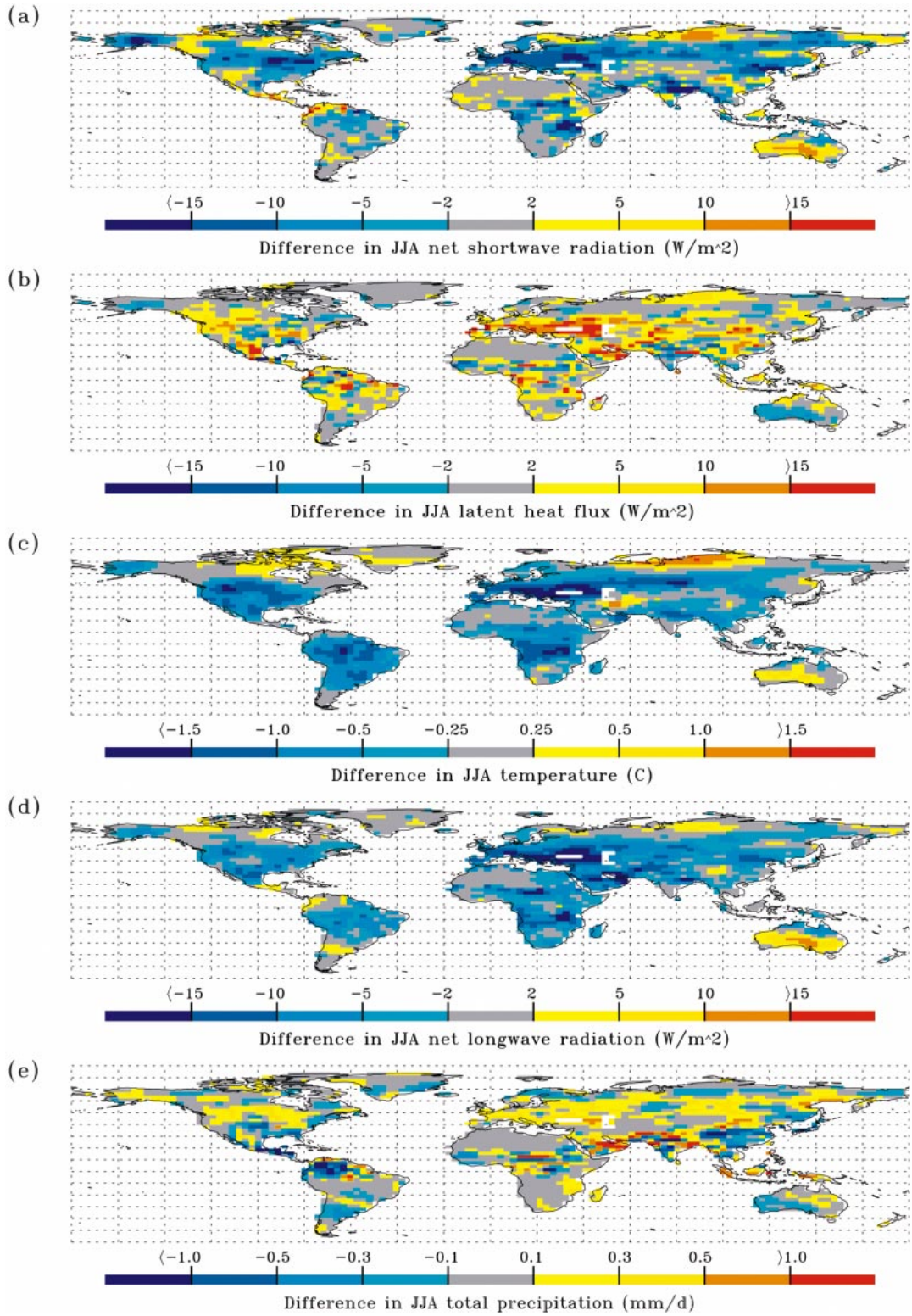


FIG. 6. Spatial pattern of 9-yr averaged differences (1982–90) between the maxLAI and minLAI simulation in JJA: (a) net shortwave flux, (b) latent heat flux, (c) near-surface temperature, (d) net longwave flux, and (e) total precipitation.

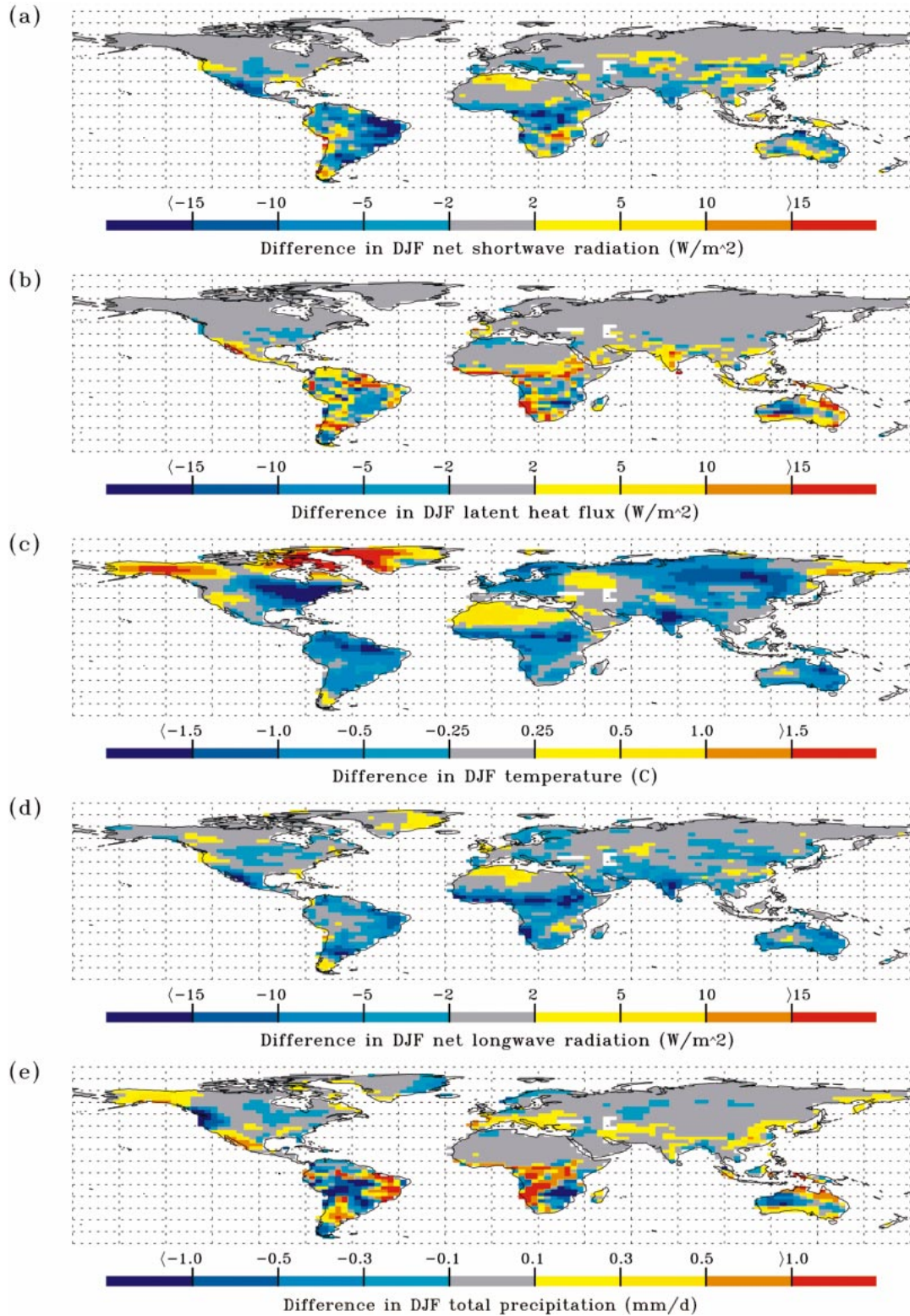


FIG. 7. Spatial pattern of 10-yr averaged differences (1981/82–1990/91) between the maxLAI and minLAI simulation in DJF: (a) net shortwave flux, (b) latent heat flux, (c) near-surface temperature, (d) net longwave flux, and (e) total precipitation.

TABLE 2. JJA differences in select near-surface climate variables (9-yr averages) between the maxLAI and minLAI simulations for the LSM surface types of cool needleleaf evergreen tree and cool grassland.

Variable		Cool needleleaf evergreen tree*		Cool grassland**	
		MaxLAI - MinLAI	% Change	MaxLAI - MinLAI	% Change
LAI range		3.5-2.0	75.0	1.4-0.6	133.3
Net shortwave flux	W m ⁻²	-5.8	-2.0	-9.4	-3.9
Albedo		0.00	0.0	+0.01	+5.0
Net longwave flux	W m ⁻²	-5.4	-4.8	-11.8	-11.5
Net radiation	W m ⁻²	-0.4	-0.2	+2.4	+1.6
Latent heat flux	W m ⁻²	+7.0	20.0	+13.7	+16.6
Canopy transpiration	W m ⁻²	+4.5	+21.9	+14.0	+97.4
Canopy evaporation	W m ⁻²	+0.5	+26.4	+1.6	+22.0
Ground evaporation	W m ⁻²	+1.9	+15.5	-1.9	-3.1
Temperature	°C	-0.80	-5.4	-1.48	-9.4
Total precipitation	mm day ⁻¹	+0.10	+20.0	+0.30	+11.6

* Cool needleleaf evergreen tree: 75% needleleaf evergreen tree, 25% bare ground, located at 45°-50.6°N and 116.7°-122.3°W.

** Cool grassland: 60% cool grass, 20% warm grass, 20% bare ground, located at 45°-50.6°N and 108.3°-113.9°W.

pendence of many canopy processes with respect to LAI (see also discussion below). Over most regions the observed increase in the latent heat flux is accompanied by an increase in precipitation. However, a few regions, for example eastern China in JJA, exhibit the opposite behavior. Here precipitation decreases with increasing evapotranspiration. In a previous sensitivity study, Pan et al. (1996) found that increasing local evapotranspiration may suppress local rainfall if the lower atmosphere is humid and lacks sufficient thermal forcing to initiate deep convection.

Decreases in net shortwave radiation, exceeding 15 W m⁻², and increases in total precipitation can be noted in large regions of temperate North America and Eurasia during JJA in the maxLAI simulation (Figs. 6a and 6e). In these regions latent heat flux increases were observed (Fig. 6b). During the austral summer, similar magnitude decreases in net shortwave radiation and increases in total precipitation are seen in the tropical regions of South America, Africa, and Australia (Figs. 7a and 7e). Generally, the albedo over densely vegetated regions is lower, which should result in an increase in net short-

wave radiation. However, our results indicate that reductions in incident solar radiation resulting from increased cloud cover, consistent with an observed increase in precipitation and evapotranspiration, overcompensate for the effects of surface albedo, leading to the observed decrease in net shortwave radiation.

Tables 2 and 3 show differences in select near-surface climate variables between the maxLAI and minLAI simulations for forested regions (high LAI) and grasslands (low LAI) in northwestern and southern North America, respectively. These differences represent spatial averages over four model grid cells for each region. In the maxLAI simulation, all sites indicate increases in the latent heat flux and precipitation, decreases in net shortwave flux, temperature and net longwave flux, and negligible changes in surface albedo. However, the changes in the surface energy budget, especially canopy transpiration, are varied depending on the vegetation type, or the base LAI, because of the nonlinear response of many canopy processes with respect to LAI. Surface albedo changes are unlikely to result from interannual LAI changes in already heavily vegetated areas, unless

TABLE 3. JJA differences in select near-surface climate variables (9-yr averages) between the maxLAI and minLAI simulations for the LSM surface types of warm forest crop and warm grassland.

Variable		Warm forest crop*		Warm grassland**	
		MaxLAI - MinLAI	% Change	MaxLAI - MinLAI	% Change
LAI range		3.7-2.0	85.0	1.6-0.6	166.7
Net shortwave flux	W m ⁻²	-3.7	-1.5	-6.8	-2.6
Albedo		+0.01	+4.1	0.00	+0.1
Net longwave flux	W m ⁻²	-4.3	-6.1	-12.3	-12.2
Net radiation	W m ⁻²	+0.6	+0.3	+5.5	+3.5
Latent heat flux	W m ⁻²	+7.8	+7.0	+21.4	+37.6
Canopy transpiration	W m ⁻²	+17.3	+39.9	+20.0	+91.0
Canopy evaporation	W m ⁻²	+1.7	+12.8	+1.4	+38.3
Ground evaporation	W m ⁻²	-11.1	-20.3	0.0	0.0
Temperature	°C	-0.78	-3.3	-1.08	-4.5
Total precipitation	mm day ⁻¹	+0.10	+3.0	+0.19	+14.1

* Warm forest crop: 40% crop, 30% broadleaf deciduous tree, 30% needleleaf evergreen tree, located at 36.6°-42.2°N and 77.4°-83.0°W.

** Warm grassland: 60% warm grass, 20% cool grass, 20% bare ground, located at 22.5°-28.1°N and 97°-102.6°W.

TABLE 4. Comparison of climate variables from the maxLAI and minLAI simulations. Values represent annual means from nine subsequent years (1982–90) of simulation data, averaged over all the land surface (60°S–80°N).

		MinLAI	MaxLAI
Solar net radiation	W m ⁻²	157.8	156.4
Thermal net radiation	W m ⁻²	-74.1	-71.1
Latent heat flux	W m ⁻²	-46.3	-48.3
Sensible heat flux	W m ⁻²	-36.1	-35.0
2-m air temperature	°C	11.96 (13.51)*	11.66 (13.43)*
Total precipitation	mm day ⁻¹	2.38	2.42

* Integration performed over entire globe.

there is a change in the fractional vegetation cover. Even though the albedo is unchanged, the fractions of energy absorbed by the vegetation and the ground below can change. Thus, it appears that the dominant impact of interannual LAI changes is modification of the partitioning of radiant energy between latent and sensible heat fluxes brought about through changes in the proportion of radiant energy absorbed by the vegetation canopy and the underlying ground, and not due to changes in surface albedo. These results also closely agree to those from a recent sensitivity study on changes in the surface energy budget from interannual changes in NDVI (Bounoua et al. 2000).

As a result of changes in the partitioning of absorbed radiant energy into sensible and latent heat fluxes, large changes in near-surface temperature are observed over large regions that can be attributed to interannual LAI variations (Figs. 6c and 7c). Cooling of more than 1°C can be noted in many regions on all the continents in the maxLAI simulation during both the boreal and austral summers. A corresponding decrease in net longwave radiation can be seen (Figs. 6d and 7d) in the maxLAI simulation, which in many regions offsets or even overcompensates for the most part the decreases in net shortwave radiation (Figs. 6a and 7a). Consequently, surface net radiation is either unchanged or only marginally increased. The large magnitude changes in surface temperature in the northern high latitudes during the DJF period could be due to variations in surface albedo ($> \pm 0.05$; not shown) possibly from changes in snow cover and masking of the dark evergreen vegetation cover, but the resulting changes on the radiation balance are not seen. Chase et al. (1996) and Zhang et al. (1996b) report that tropical and midlatitude vegetation forcing can cause long-ranging effects in the high-latitude climates. Changes in the atmospheric heating pattern in the Tropics from variations in latent heat activity may modify the Hadley circulation, which then may alter the generation of waves along the polar front (Chase et al. 1996).

Table 4 shows annual means of select climate variables for all land between 60°S to 80°N. Near-surface temperature in the maxLAI scenario is cooler by about 0.3°C when compared with the minLAI scenario (with

oceans, the difference is only 0.08°C). Absorbed solar energy over land changes by less than 1% between the two cases. In fact, our analysis shows that land albedo remains nearly constant at about 0.2. Although the amount of radiant energy absorbed may be similar in both minLAI and maxLAI simulations, the portions absorbed by the vegetation canopy and the underlying ground are different, depending on the LAI change. The decrease in net solar radiation is due to more cloud cover over land in the maxLAI simulation. Latent heat flux increased by 4.3% and sensible heat decreased by 3% in the maxLAI simulation. Total precipitation increased by 1.7% in the maxLAI scenario, consistent with an increase in latent heat flux and more cloud cover. These results confirm previously reported impacts of LAI changes on the near-surface climate, although no where near as dramatic as simulations that removed large tracts of vegetation (e.g., Nobre et al. 1991; Bonan et al. 1992) or even the entire planetary vegetation (Kleidon et al. 2000).

3) STATISTICAL SIGNIFICANCE

In order to establish statistical significance of the observed differences in time averages of the temperature and precipitation fields between the two simulations, a local *t* test was performed (Wigley and Santer 1990). Table 5 shows seasonal and zonal mean differences in surface temperature (2-m height) and total precipitation over land between the maxLAI and minLAI model runs. Surface temperatures were cooler by about 0.4°C during JJA and precipitation increased by 0.05 mm day⁻¹ in the maxLAI simulation. The temperate band and southern Tropics contribute most to this cooling and increased rainfall. During the austral summer, temperatures were cooler by about 0.3°C and precipitation increased also by 0.05 mm day⁻¹ in the maxLAI simulation, with contributions mostly from the Tropics and Southern Hemisphere. Overall, about 32% (JJA) and 22% (DJF) of all land points (including vegetated and nonvegetated areas) show statistically significant differences (10% level) in the temperature time means between the two model runs. In contrast, the differences in the precipitation time means are less statistically significant. The meridional distribution of the differences in zonal mean surface temperatures during the boreal and austral summers compare well to those reported by Bounoua et al. (2000). The remaining differences in these fields might be explained in part through small differences in vegetation forcing, model sensitivity and effects of climatological SST (Bounoua et al. 2000) versus observed SST (this study) as boundary forcing.

Station temperature records indicate an increase of global mean land surface temperature by about 0.8°C during the past century (Hansen et al. 1999); therefore, temperature differences on the order of 0.3°–0.4°C caused by interannual LAI changes are not insignificant.

TABLE 5. Seasonal and zonal mean differences in near-surface temperature (2-m height) and total precipitation over land between the maxLAI and minLAI simulations. Values for JJA are based on 9 yr (1982–90) and for DJF on 10 yr (1981/82–1990/91) of simulation data.

Zonal band (No. of pixel)	Area m ²	JJA MaxLAI–MinLAI				DJF MaxLAI–MinLAI			
		Temperature		Precipitation		Temperature		Precipitation	
		°C	(10%)*	mm day ⁻¹	(10%)	°C	(10%)	mm day ⁻¹	(10%)
All land**	1.36 × 10 ¹⁴	-0.39	31.6	+0.05	8.5	-0.31	21.9	+0.05	9.8
60°–80°N (546)	1.95 × 10 ¹³	+0.09	10.3	+0.04	5.3	+0.22	4.2	+0.02	7.5
40°–60°N (491)	3.11 × 10 ¹³	-0.62	44.4	+0.11	7.1	-0.49	9.6	-0.01	11.0
23°–40°N (316)	2.64 × 10 ¹³	-0.39	32.6	+0.02	10.8	-0.13	17.7	+0.06	6.3
0°–23°N (262)	2.49 × 10 ¹³	-0.36	36.3	-0.03	10.3	-0.40	39.3	+0.08	6.9
23°S–0° (232)	2.21 × 10 ¹³	-0.65	57.8	+0.10	11.6	-0.55	62.5	+0.13	19.0
60°–23°S (152)	1.26 × 10 ¹³	-0.13	17.1	-0.01	11.8	-0.43	42.1	+0.01	12.5

* Fraction (%) of locally successful pixels, meaning local difference in mean temperature is statistically significant to the 10% confidence level.

** 60°S–80°N.

Furthermore, the temperature differences in some regions are much larger, many times exceeding 1°C.

4. Concluding remarks

In this study we evaluated the utility of satellite-based LAI data in improving the simulation of near-surface climate in NCAR CCM3 global climate model. First, we performed a control run with standard LSM LAI profiles and a case run with 10-yr (Jul 1981–Jun 1991) average monthly mean LAI profiles derived from satellite data. Regional differences in the simulated near-surface climate between the two runs indicate a substantial warming and decrease in precipitation during the boreal summer over large parts of the Northern Hemisphere lands in the satellite LAI run. Such warming and decreased precipitation, attributable to the lower magnitudes of satellite LAI data, reduced the model biases in near-surface temperature and precipitation in comparison to observations. In particular, the near-surface temperature over grasslands during the active growing season in both hemispheres is consistently better simulated with satellite LAI data. In summary, usage of satellite LAI leads to an improvement in the near-surface temperature and precipitation simulations over certain regions. However, significant residual cold biases remain. It has been speculated that modeled processes in the atmosphere, prescribed surface albedos of bare soil and thick canopy (stomatal resistance too small) in the CCM3–LSM scheme are primarily responsible for the cold bias.

Second, we investigated the impact of interannual vegetation extremes observed during the 1980s on near-surface climate by utilizing the maximum and minimum LAI values from the 10-yr LAI record. Analysis of the surface energy budget indicates notable increases in latent heat flux in the greener scenario over large vegetated temperate areas of North America and Eurasia during the boreal summer. Similar increases were seen in the southern continents during the austral summer.

These correspond well to observed LAI variations. Reductions in net shortwave flux were observed over regions of increased latent heat activity mainly due to a change in cloud cover, consistent with an observed increase in precipitation, and not surface albedo. Annual near-surface air temperatures decreased by about 0.3°C and annual total precipitation increased by 0.04 mm day⁻¹ when averaged over all land area. Broadleaf evergreen forests in the Tropics and temperate grasslands during the boreal summer contribute most to this cooling and increased rainfall. The corresponding reduction in net longwave flux balanced or overcompensated for the most part the decrease in net shortwave flux. Consequently, the total available radiant energy at the surface was either unchanged or only marginally increased. It thus appears that the dominant impact of interannual LAI variations is modification of the partitioning of net radiant energy between latent and sensible heat fluxes brought about through changes in the proportion of energy absorbed by the vegetation canopy and the underlying ground and not from surface albedo changes.

Together, these results illustrate the importance of vegetation LAI changes on near-surface climate variations. An important shortcoming of the present study is the use of vegetation-specific LAI profiles rather than observed LAI data by model grid cell, as in the case of SSTs. The latter facilitates inclusion of spatial information inherent in the satellite product. To do this, however, requires a significant reformulation of the existing model structures in LSM. The Common Land Model activity currently underway addresses this issue. Therefore, the next generation of models will facilitate linkages not only with satellite LAI fields, but also with other key variables such as roughness length and fractional vegetation cover, thus greatly increasing the realism of surface prescription.

Acknowledgments. This research was funded by NOAA/NASA Enhanced Dataset Program Grant

NA76GP0481 (PI: Myneni) and NASA IDS Grant (PI: Dickinson).

REFERENCES

- Bastable, H. G., W. J. Shuttleworth, R. L. G. Dallara, G. Fisch, and C. A. Nobre, 1993: Observations of climate, albedo and surface radiation over cleared and undisturbed amazonia forest. *Int. J. Climatol.*, **13**, 783–796.
- Betts, A. K., and A. C. M. Beljaars, 1993: Estimation of effective roughness length for heat and momentum from FIFE data. *Atmos. Res.*, **30**, 251–261.
- , J. H. Ball, A. C. M. Beljaars, M. J. Miller, and P. A. Viterbo, 1996: The land surface–atmosphere interaction: A review based on observational and global modeling perspectives. *J. Geophys. Res.*, **101**, 7209–7225.
- , M. Goulden, and S. Wofsy, 1999: Controls on evaporation in a boreal spruce forest. *J. Climate*, **12**, 1601–1618.
- Bonan, G. B., 1996: A Land Surface Model (LSM version 1.0) for ecological, hydrological, and atmospheric studies: Technical description user's guide. NCAR Tech. Note NCAR/TN-417+STR, National Center for Atmospheric Research, Boulder, CO, 150 pp. [Available from NCAR, P.O. Box 3000, Boulder, CO 80307.]
- , 1998: The land surface climatology of the NCAR Land Surface Model coupled the NCAR Community Climate Model. *J. Climate*, **11**, 1307–1327.
- , D. Pollard, and S. L. Thompson, 1992: Effects of boreal forest vegetation on global climate. *Nature*, **359**, 716–718.
- Bounoua, L., G. J. Collatz, S. O. Los, P. J. Sellers, D. A. Dazlich, C. J. Tucker, and D. A. Randall, 2000: Sensitivity of climate to changes in NDVI. *J. Climate*, **13**, 2277–2292.
- Chalita, S., and H. Le Treut, 1994: The albedo of temperate and boreal forest and the northern-hemisphere climate—A sensitivity experiment using the LMD-GCM. *Climate Dyn.*, **10**, 231–240.
- Chase, T. N., R. A. Pielke, T. G. F. Kittel, R. Nemani, and S. W. Running, 1996: Sensitivity of a general circulation model to global changes in leaf area index. *J. Geophys. Res.*, **101**, 7393–7408.
- Collatz, G., J. Ball, C. Grivet, and J. A. Berry, 1991: Physiological and environmental regulation of stomatal conductance, photosynthesis and transpiration: A model that includes a laminar boundary layer. *Agric. For. Meteorol.*, **54**, 107–136.
- Dickinson, R. E., 1983: Land surface processes and climate–surface albedos and energy balance. *Advances in Geophysics*, Vol. 25, Academic Press, 305–353.
- , and A. Henderson-Sellers, 1988: Modeling tropical deforestation: A study of GCM land-surface parameterizations. *Quart. J. Roy. Meteor. Soc.*, **114**, 439–462.
- Hansen, J., R. Ruedy, J. Glascoe, and M. Sato, 1999: GISS analysis of surface temperature change. *J. Geophys. Res.*, **104**, 30 997–31 022.
- Henderson-Sellers, A., K. McGuffie, and C. Gross, 1995: Sensitivity of global climate model simulations to increased stomatal resistance and CO₂ increases. *J. Climate*, **8**, 1738–1756.
- Hulme, M., T. J. Osborn, and T. C. Johns, 1998: Precipitation sensitivity to global warming: Comparison of observations with HadCM2 simulations. *Geophys. Res. Lett.*, **25**, 3379–3382.
- Hutjes, R. W. A., and Coauthors, 1998: Biospheric aspects of the hydrological cycle—Preface. *J. Hydrol.*, **213**, 1–21.
- Jones, P. D., M. New, D. E. Parker, S. Martin, and I. G. Rigor, 1999: Surface air temperature and its changes over the past 150 years. *Rev. Geophys.*, **37**, 173–199.
- Kiehl, J., J. Hack, G. B. Bonan, B. Bonville, B. Briegleb, D. Williamson, and P. Rasch, 1996: Description of the NCAR Community Climate Model (CCM3). Tech. Rep. NCAR/TN-420+STR, National Center for Atmospheric Research, Boulder, CO, 152 pp. [Available from NCAR, P.O. Box 3000, Boulder, CO 80307.]
- , —, —, —, —, D. L. Williamson, and P. J. Rasch, 1998: The National Center for Atmospheric Research Community Climate Model: CCM3. *J. Climate*, **11**, 1131–1149.
- Kleidon, A., K. Fraedrich, and M. Heimann, 2000: A green planet versus a desert world: Estimating the maximum effect of vegetation on the land surface climate. *Climatic Change*, **44**, 471–493.
- Lean, J., and D. A. Warrilow, 1989: Simulation of the regional climatic impact of Amazon deforestation. *Nature*, **342**, 411–413.
- LeMone, M. A., and Coauthors, 2000: Land–atmosphere interaction research, early results, and opportunities in the Walnut River Watershed in southeast Kansas: CASES and ABLE. *Bull. Amer. Meteor. Soc.*, **81**, 757–779.
- Martin, M., R. E. Dickinson, and Z. L. Yang, 1999: Use of coupled land surface general circulation model to examine the impacts of stomatal resistance on the water resources of the American Southwest. *J. Climate*, **12**, 3359–3375.
- Myneni, R. B., R. R. Nemani, and S. W. Running, 1997: Estimation of global leaf area index and absorbed par using radiative transfer models. *IEEE Trans. Geosci. Remote Sens.*, **35**, 1380–1393.
- Nobre, C. A., P. J. Sellers, and J. Shukla, 1991: Amazonian deforestation and regional climate change. *J. Climate*, **4**, 957–988.
- Olson, J. S., J. A. Watts, and L. J. Allison, 1983: Carbon in live vegetation of major world ecosystems. ORNL-5862, Oak Ridge National Laboratory, Oak Ridge, TN, 180 pp.
- Pan, Z. T., E. Takle, M. Segal, and R. Turner, 1996: Influences of model parameterization schemes on the response of rainfall to soil moisture in the central United States. *Mon. Wea. Rev.*, **124**, 1786–1802.
- Pielke, R. A., R. Avissar, M. Raupach, A. J. Dolman, Y. Xeng, and S. Denning, 1998: Interactions between the atmosphere and terrestrial ecosystems: Influence on weather and climate. *Global Change Biol.*, **4**, 461–475.
- Pollard, D., and S. L. Thompson, 1995: Use of a land-surface transfer scheme (LSX) in a global climate model: The response to doubling stomatal resistance. *Global Planet. Change*, **10**, 129–162.
- Schwartz, M. D., and T. R. Karl, 1990: Spring phenology: Nature's experiment to detect the effect of “green up” on surface maximum temperatures. *Mon. Wea. Rev.*, **118**, 883–890.
- Sellers, P. J., 1985: Canopy reflectance, photosynthesis and transpiration. *Int. J. Remote Sens.*, **6**, 1335–1372.
- , J. A. Berry, G. J. Collatz, C. B. Field, and F. G. Hall, 1992: Canopy reflectance, photosynthesis, and transpiration. III. A reanalysis using improved leaf models and a canopy integration scheme. *Remote Sens. Environ.*, **42**, 187–216.
- , and Coauthors, 1995: The Boreal Ecosystem–Atmosphere Study (BOREAS): An overview and early results from the 1994 field year. *Bull. Amer. Meteor. Soc.*, **76**, 1549–1577.
- , and Coauthors, 1996: Comparison of radiative and physiological effects of doubled atmospheric CO₂ on climate. *Science*, **271**, 1402–1406.
- Shukla, J., and Y. Mintz, 1982: The influence of land-surface evapotranspiration on the earth's climate. *Science*, **247**, 1322–1325.
- Shuttleworth, W. J., J. H. C. Gash, J. M. Roberts, C. A. Nobre, L. C. B. Molion, and M. D. G. Ribeiro, 1991: Post-deforestation amazonian climate: Anglo-Brazilian research to improve prediction. *J. Hydrol.*, **129**, 71–85.
- Sud, Y. C., and M. Fennessey, 1982: A study of the influence of surface albedo on July circulation in semi-arid regions using the CLAS GCM. *J. Climatol.*, **2**, 105–128.
- , J. Shukla, and Y. Mintz, 1988: Influence of land-surface roughness on atmospheric circulation and precipitation: A sensitivity study with a general circulation model. *J. Appl. Meteor.*, **27**, 1036–1054.
- Wigley, T. M. L., and B. D. Santer, 1990: Statistical comparison of spatial fields in model validation, perturbation, and predictability experiments. *J. Geophys. Res.*, **95**, 851–886.
- Zhang, H., A. Henderson-Sellers, and K. McGuffie, 1996a: Impacts of tropical deforestation. Part I: Process analysis of local climatic change. *J. Climate*, **9**, 1497–1517.
- , K. McGuffie, and A. Henderson-Sellers, 1996b: Impacts of tropical deforestation. Part II: The role of large-scale dynamics. *J. Climate*, **9**, 2498–2521.